




To cite this article: Chunwei Zhang, Huidong Cao, A. Eyvazian, Afrasyab Khan, Naeim Farouk & Pooya Sareh (2021): Flexural wave dispersion characteristics of imperfect Ti-6Al-4V foam circular cylindrical shells in a thermal environment, *Waves in Random and Complex Media*, DOI: 10.1080/17455030.2021.1917791

# Flexural wave dispersion characteristics of imperfect Ti-6Al-4V foam circular cylindrical shells in a thermal environment

Chunwei Zhang <sup>a</sup>, Huidong Cao<sup>a</sup>, A. Eyvazian<sup>a,b</sup>, Afrasyab Khan <sup>c</sup>,  
Naeim Farouk <sup>d</sup> and Pooya Sareh<sup>e</sup>

<sup>a</sup>Structural Vibration Control Group, Qingdao University of Technology, Qingdao, People's Republic of China;

<sup>b</sup>Department of Mechanical Engineering, Polytechnic University of Milan, Milan, Italy; <sup>c</sup>Research Institute of Mechanical Engineering, Department of Vibration Testing and Equipment Condition Monitoring, South Ural State University, Chelyabinsk, Russian Federation; <sup>d</sup>Mechanical Engineering Department, College of Engineering, Prince Sattam bin Abdulaziz University, Alkharj, Saudi Arabia; <sup>e</sup>Department of Mechanical, Materials and Aerospace Engineering, University of Liverpool, Liverpool, UK

## ABSTRACT

The present paper is mainly focused on analyzing the flexural wave dispersion of imperfect Ti-6Al-4V foam circular cylindrical shells in a thermal environment. The pores were supposed to be distributed across the thickness ( $z$ -direction) in the form of three different patterns as follows: symmetric porosity distribution (SPD), asymmetric porosity distribution (ASPD) and uniform porosity distribution (UPD). Besides, various kinds of temperature variations, including sinusoidal, linear and uniform temperature variations, were studied. The strain-displacement relationship of the shell was derived based on the first-order shear deformable theory (FSDT) of shells. Hamilton's principle was also applied to obtain the governing equations of metal foam shells which were then solved using an analytical method. Finally, influences of different parameters including circumferential wave number, different kinds of temperature variation, temperature change, radius to thickness ratio  $R/h$ , types of porosity distribution across the thickness, porosity coefficient and mode number on the variations of phase velocity and wave frequency were investigated and the results were illustrated and discussed.

## KEYWORDS

Wave dispersion analysis; metal foam circular cylindrical shell; first-order shear deformable theory; porosity distribution pattern

## Introduction

One of the essential parameters in the design and analysis of structures is the weight of their constitutive materials. Various lightweight materials have been widely exploited for numerous engineering applications owing to their favorable properties. Porous materials such as metal foams, ceramic foams and graphene foams are among the most ubiquitous classes of lightweight materials with diverse applications in the automotive, aerospace, marine and civil engineering industries. For instance, aluminum foams have been utilized for energy absorption to reduce the structural mass of vehicles in the automotive industry [1,2]. A

metal foam is a cellular structure consisting of solid metal with gas-filled pores, which comprise a large portion of its volume. As such a structure is typically strong and lightweight, the mechanical properties of porous materials have been the focus of numerous investigations over the last two decades [3–5]. More specifically, porous functionally graded materials (FGMs) are considered to be generally desirable in terms of structural mass; hence analyzing their mechanical behavior has been an interesting topic for scientists and engineers. For example, the dynamic response of doubly-curved nanosize shells made of porous FGMs based on the nonlocal strain gradient theory (NSGT) was analyzed by Karami, Shahsavari [6]. Furthermore, the influence of imperfections on the vibrational behavior of FGMs tapered nanoscale beams and plates in a thermal environment according to NSGT was surveyed by Karami, Janghorban [7], Karami, Shahsavari [8].

Owing to their high melting points, titanium foams can be used in applications such as heat exchangers and catalyst substrates with temperatures up to 400°C. Moreover, titanium foams and titanium alloy foams have been utilized as structural elements in load-bearing sandwich cores for aerospace and transportation applications. Also, low density, superb biocompatibility and good corrosion resistance are some desirable properties of titanium alloy foams (e.g. Ti-6Al-4V) which make them of great interest in the biomedical industry for applications such as implants. In electrolytic equipment, to generate sodium hydroxide and chlorine by the electrolysis of aqueous sodium chloride, titanium-based electrodes have been used [9–11]. Porous titanium alloys (e.g. Ti-6Al-4V) are also preferred in the biomedical industry due to the formation of a passive TiO<sub>2</sub> layer when in contact with oxidizing environments.

In addition, many recent studies considered the engineering properties and behavior of metal foam structures. For instance, the stability, static, and free and forced dynamic characteristics of imperfect metal foam Timoshenko beams were discussed by Chen, Yang [12], Chen, Yang [13]. Wang and Wu [14] investigated the influence of various boundary conditions on the vibrational response of a metal foam shell based on the Rayleigh-Ritz method in conjunction with the sinusoidal shear deformable model. Considering graphene platelets (GPLs), Kitipornchai, Chen [15] also studied the dynamic and buckling behaviors of GPLs-reinforced metal foam beams where the internal pores and nanofillers are distributed either uniformly and non-uniformly in various metal matrices including titanium, aluminum, magnesium, copper and nickel matrices. Forced vibrational analysis of nanoscale plates of porous metal foam lying on an elastic foundation was explored by Barati [16] based on the 4-variable plate theory and NSGT. Barati and Zenkour [17] used Galerkin's method to solve the post-buckling problem of porous metal foam nanoscale beams in the framework of the nonlocal nonlinear refined shear deformable beam theory. Stability and natural frequency characteristics of graphene-reinforced porous metal foam plates were assessed by Yang, Chen [18] based on the Chebyshev-Ritz method. Eringen's nonlocal elasticity theory was also employed by Wang and Zhang [19] to examine the stability of metal foam refined nanoplates using the Navier solution method. Gao, Gao [20] performed a nonlinear vibration analysis on plates made of GPLs-reinforced metal foam lying on an elastic substrate with various boundary conditions using the differential quadrature method. The effect of spinning motion on the natural frequency of graphene-reinforced metal foam cylindrical shells was investigated by Dong, Li [21] according to the first-order shear deformable theory (FSDT). Fenjan, Ahmed [22] conducted a vibration analysis on the double-coupled imperfect

metal foam nanoscale plate rested on an elastic medium based on NSGT. Moreover, Wang, Ye [23] studied the nonlinear dynamic response of GPL-reinforced metal foam circular cylindrical shells according to the modified Donnell nonlinear shell theory. In another attempt, Wang, Liu [24] utilized Navier's solution and Galerkin's method to solve the vibrational problem of metal foam cylindrical nanoshells under different boundary conditions using the modified couple stress theory (MCST) in conjunction with Love's thin shell theory. The dynamic analysis of metal foam cylindrical microscale shells in contact with a moving load was presented by Mirjavadi, Forsat [25] based on the shell FSDT. The same method was also implemented by Zhang and Zhang [26] to probe the vibration and buckling responses of nanoshells made of nanoporous metal foam utilizing Navier's solution. In addition, the nonlinear vibrational behavior of nanoscale thick metal foam beams on a nonlinear foundation was surveyed by Alasadi, Ahmed [27] according to Eringen's nonlocal elasticity theory. Lately, Liu and Wang [28] discussed the dynamics and stability of 3D graphene foam microshells whose pores were considered to be distributed either uniformly or non-uniformly according to Love's thin shell theory and MCST, respectively. Propagation of waves in metal foam rectangular plates with graded porosities lying on Kerr's foundation in a thermal environment based on the refined higher-order plate theory was analyzed by Ebrahimi and Seyfi [29].

In the context of imperfect metal foams, wave propagation analysis is one of the most significant mechanical analyzes which has been less surveyed in scientific papers. Hence, it is necessary to inspect such structures in the framework of wave propagation analysis [30–33]. For instance, Karami, Shahsavari [34] used the bi-Helmholtz NSGT to solve the wave dispersion problem of an embedded viscoelastic single-layer graphene sheet under an in-plane magnetic field in a hygrothermal environment. She, Yuan [35] examined thermal effects on wave dispersion behaviors, including the longitudinal, shear and flexural waves of porous FGM nanotubes based on NSGT. Ayache, Bennai [36] also investigated wave propagations and vibrations in beams consisted of porous FGM on the basis of high-order hyperbolic shear deformable theory. The influence of an in-plane magnetic field on the propagation of waves within an embedded nanosize plate made of imperfect FGMs was explored by Karami, Shahsavari [37] based on the second-order shear deformation theory and NSGT. Wave dispersion in an FG porous nanobeam and nanoplate was examined by Ebrahimi, Seyfi [38], Ebrahimi, Seyfi [39] in the framework of refined higher-order shear deformable beam and plate theories in conjunction with NSGT. Furthermore, Ebrahimi, Seyfi [38] studied the flexural wave propagation in a GPLs-reinforced metal matrix nanocomposite considering the porosity effect within the framework of FSDT. Wang and Liang [40] presented wave propagation analysis of the Euler-Bernoulli and Timoshenko nanobeams made of nanoporous metal foams on the basis of Eringen's nonlocal theory. A quasi-3D refined plate theory was implemented by Sobhy and Zenkour [41] in conjunction with NSGT to study the wave dispersion behavior in an embedded bi-layer porous FG nanoplates subjected to an in-plane 2D-magnetic field. Lately, Faroughi, Rahmani [42] probed the wave propagation characteristics of a bi-dimensional porous FGM nanobeam taking into account the impact of rotation based on Reddy's beam theory. In order to solve wave propagation problems, an analytical method is implemented, which consists of a harmonic solution. By utilizing this solution procedure, far from any boundary condition, the behavior of wave propagation can be analyzed. The literature review, however,

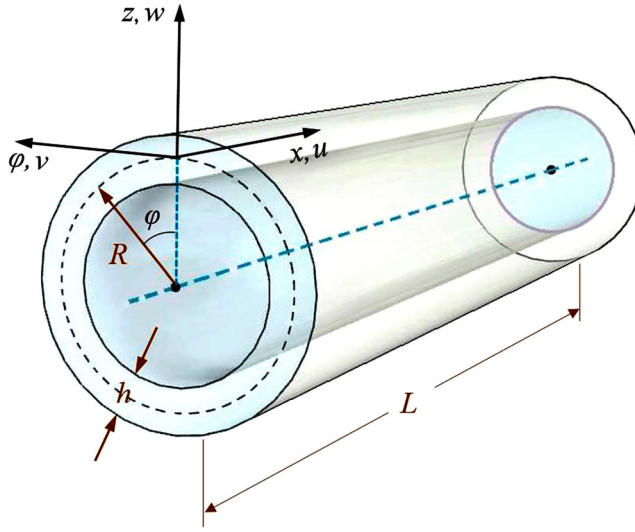


**Figure 1.** Coordinate system and geometry of a typical cylindrical shell.

showed no study addressing the wave propagation of metal foam shells in thermal environments. Thus, the present paper is aimed at filling this gap by presenting the results of an investigation on the dispersion of flexural waves in metal foam shells in a thermal environment for the first time. Three various porosity distribution patterns were considered. Besides, the cylindrical shell was modeled by FSDT, and Hamilton's principle was implemented to determine motion equations. Subsequently, a harmonic solution method was applied to solve the obtained governing equations. The influence of various variables on the phase velocity and wave frequency of shells made of imperfect metal foam was explored and presented.

## Theoretical basis and problem formulation

The geometry and the coordinate system of a metal foam circular cylindrical shell are depicted in Figure 1, where the radius, length, and thickness of the cylindrical shell are denoted by  $R$ ,  $L$  and  $h$ , respectively.

Three different uniform and non-uniform porosity distribution patterns were considered to evaluate their influence on the corresponding properties of imperfect metal foam. The illustration of the distribution of pores across the shell thickness can be found in Figure 2 [12,17,43,44].

The equivalent properties of a uniformly imperfect metal foam can be calculated by the following equations:

$$E(z) = E_1(1 - \xi \chi) \quad (1)$$

$$\alpha(z) = \alpha_1(1 - \xi \chi) \quad (2)$$

$$\rho(z) = \rho_1 \sqrt{1 - \xi \rho \chi} \quad (3)$$

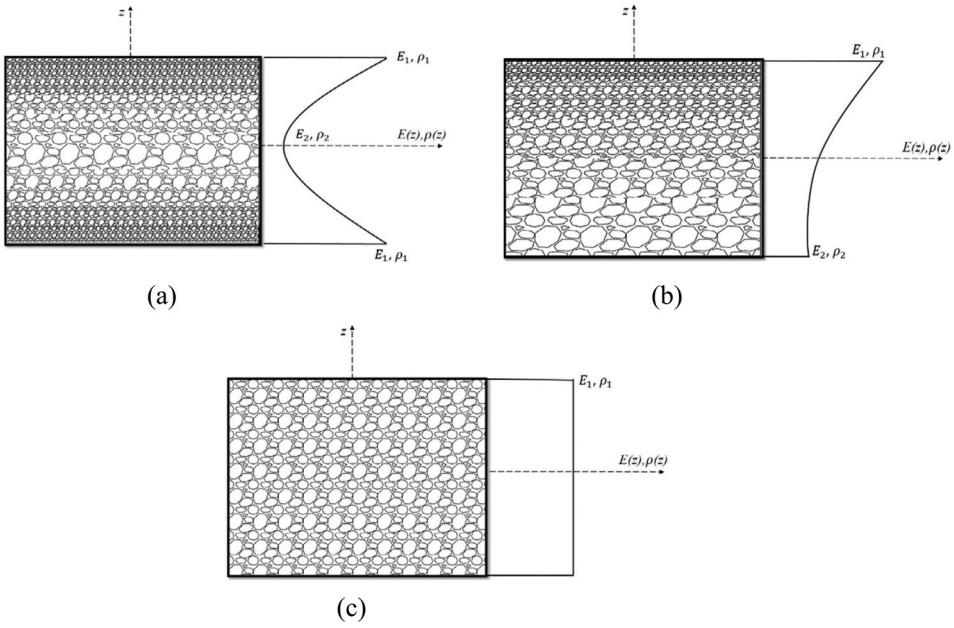


**Figure 2.** Schematic representation of different porosity distributions across the shell thickness for (a) symmetric porosity distribution, (b) asymmetric porosity distribution and (c) uniform porosity distribution [29].

The term  $\lambda$  in Equations (1)–(3) can be expressed as follows:

$$\chi = \frac{1}{\xi} - \frac{1}{\xi} \left[ \frac{2}{\pi} \left( \sqrt{1-\xi} - 1 \right) + 1 \right]^2 \quad (4)$$

Besides, two patterns were considered for non-uniform distribution of pores: symmetric and asymmetric. The equivalent properties of the asymmetrically imperfect metal foam are determined by:

$$E(z) = E_1 \left( 1 - \xi \cos \left( \frac{\pi z}{h} \right) \right) \quad (5)$$

$$\alpha(z) = \alpha_1 \left( 1 - \xi \cos \left( \frac{\pi z}{h} \right) \right) \quad (6)$$

$$\rho(z) = \rho_1 \left( 1 - \xi_\rho \cos \left( \frac{\pi z}{h} \right) \right) \quad (7)$$

Also, the above equations can be determined for the asymmetric porosity distribution as follow:

$$E(z) = E_1 \left( 1 - \xi \cos \frac{\pi}{2} \left( \frac{z}{h} + \frac{1}{2} \right) \right) \quad (8)$$

$$\alpha(z) = \alpha_1 \left( 1 - \xi \cos \frac{\pi}{2} \left( \frac{z}{h} + \frac{1}{2} \right) \right) \quad (9)$$

$$\rho(z) = \rho_1 \left( 1 - \xi_\rho \cos \frac{\pi}{2} \left( \frac{z}{h} + \frac{1}{2} \right) \right) \quad (10)$$

where  $E(z)$ ,  $\alpha(z)$  and  $\rho(z)$  denotes Young's modulus, thermal expansion coefficient, and mass density across the thickness of the imperfect metal foam cylindrical shell, respectively. In the current method, as the variation of Poisson's ratio is very small, it can be taken into account as a constant. In addition, the porosity coefficient ( $\xi$ ) can be formulated as:

$$\xi = 1 - \frac{E_2}{E_1} = 1 - \frac{G_2}{G_1} \quad (11)$$

Also, density coefficient ( $\xi_\rho$ ) can be formulated as:

$$\xi_\rho = 1 - \frac{\rho_2}{\rho_1} \quad (12)$$

where  $E_1$ ,  $\alpha_1$  and  $\rho_1$  represents the maximum values of Young's modulus, thermal expansion coefficient, and mass density of the imperfect metal foam, respectively. Similarly,  $E_2$ ,  $\alpha_2$  and  $\rho_2$  represents the minimum values of the aforementioned parameters. It is worth noting that the porosity coefficient and also density coefficient vary between 0 and 1. On the other hand, such coefficients cannot take values greater than 1. Moreover, there is a relation between Young's modulus and mass density for open-cell metal foams as follows:

$$\frac{\rho_2}{\rho_1} = \sqrt{\frac{E_2}{E_1}} \quad (13)$$

By using this relation, density coefficient (Equation (12)) can be rewritten as:

$$\xi_\rho = 1 - \sqrt{\frac{E_2}{E_1}} \quad (14)$$

By substituting Equation (11) into Equation (14), the following equation can be obtained that in the framework of this equation, porosity coefficient and density coefficient are related together.

$$\xi_\rho = 1 - \sqrt{1 - \xi} \quad (15)$$

The following equation states the stress-strain relationship of imperfect metal foam:

$$\sigma_{ij} = C_{ijkl}(\varepsilon_{kl} - \alpha_{ij}\Delta T) \quad (16)$$

where  $\sigma_{ij}$  stands for Cauchy stress components,  $\varepsilon_{kl}$  is strain tensor components,  $C_{ijkl}$  denotes elasticity tensor components,  $\alpha_{ij}$  is thermal expansion tensor components and finally,  $\Delta T$  denotes temperature change.

Based on the former investigations, which were considering thermal environments, the effects of various kinds of temperature variation or thermal loading called uniform temperature variation (UTV), linear temperature variation (LTV) and sinusoidal temperature variation (STV) on the behavior of propagated waves has been examined in the current investigation. The initial temperature was regarded to be room temperature  $T_0 = 300\text{K}$ . The final

temperature ( $T$ ) of various types of temperature rise can be formulated as [45]:

$$\begin{cases} T = T_0 + \Delta T \left( \frac{1}{2} + \frac{z}{h} \right) \text{ LTV} \\ T = T_0 + \Delta T \left( 1 - \cos \frac{\pi}{2} \left( \frac{1}{2} + \frac{z}{h} \right) \right) \text{ STV} \\ T = T_0 + \Delta T \text{ UTV} \end{cases} \quad (17)$$

According to FSDT, the motion relations of a shell can be stated in the following form [46]:

$$u_x(x, \phi, z, t) = u(x, \phi, t) + z\theta_x(x, \phi, t) \quad (18)$$

$$u_\phi(x, \phi, z, t) = v(x, \phi, t) + z\theta_\phi(x, \phi, t) \quad (19)$$

$$u_z(x, \phi, z, t) = w(x, \phi, t) \quad (20)$$

where  $u$  denotes axial displacement,  $v$  denotes circumferential displacement and  $w$  denotes lateral displacement. Additionally,  $\theta_\phi$  and  $\theta_x$  illustrates the circumferential and axial rotation components. Therefore, the following equation presents the nonzero strains of a shell:

$$\varepsilon_{xx} = \frac{\partial u}{\partial x} + z \frac{\partial \theta_x}{\partial x} \quad (21)$$

$$\varepsilon_{\phi\phi} = \frac{1}{R} \left( w + \frac{\partial v}{\partial \phi} + z \frac{\partial \theta_\phi}{\partial \phi} \right) \quad (22)$$

$$\varepsilon_{xz} = \theta_x + \frac{\partial w}{\partial x} \quad (23)$$

$$\varepsilon_{x\phi} = \frac{\partial v}{\partial x} + \frac{1}{R} \frac{\partial u}{\partial \phi} + \frac{z}{R} \frac{\partial \theta_x}{\partial \phi} + z \frac{\partial \theta_\phi}{\partial x} \quad (24)$$

$$\varepsilon_{\phi z} = \theta_\phi + \frac{1}{R} \frac{\partial w}{\partial \phi} - \frac{v}{R} \quad (25)$$

Thereupon, to attain Euler-Lagrange equations of metal foam shells, Hamilton's principle is employed:

$$\int_{t_0}^{t_1} [\delta U - \delta K - \delta W_{nc}] dt = 0 \quad (26)$$

where  $U$  denotes strain energy,  $K$  is kinetic energy and  $W_{nc}$  represents work done by the non-conservative external loads. The variation of strain energy can be stated as follow:

$$\begin{aligned} \delta U &= \int_{-\frac{h}{2}}^{\frac{h}{2}} \int_0^{2\pi} \int_0^L \sigma_{ij} \delta \varepsilon_{ij} R dx d\phi dz \\ &= \int_{-\frac{h}{2}}^{\frac{h}{2}} \int_0^{2\pi} \int_0^L [\sigma_{xx} \delta \varepsilon_{xx} + \sigma_{\phi\phi} \delta \varepsilon_{\phi\phi} + \sigma_{xz} \delta \varepsilon_{xz} + \sigma_{x\phi} \delta \varepsilon_{x\phi} + \sigma_{\phi z} \delta \varepsilon_{\phi z}] R dx d\phi dz \\ &= \int_{-\frac{h}{2}}^{\frac{h}{2}} \int_0^{2\pi} \int_0^L \left[ \begin{aligned} &\sigma_{xx} \delta \left( \frac{\partial u}{\partial x} + z \frac{\partial \theta_x}{\partial x} \right) + \sigma_{\phi\phi} \delta \left( \frac{1}{R} \left( w + \frac{\partial v}{\partial \phi} + z \frac{\partial \theta_\phi}{\partial \phi} \right) \right) \\ &+ \sigma_{xz} \delta \left( \theta_x + \frac{\partial w}{\partial x} \right) + \sigma_{x\phi} \delta \left( \frac{\partial v}{\partial x} + \frac{1}{R} \frac{\partial u}{\partial \phi} + \frac{z}{R} \frac{\partial \theta_x}{\partial \phi} + z \frac{\partial \theta_\phi}{\partial x} \right) \\ &+ \sigma_{\phi z} \delta \left( \theta_\phi + \frac{1}{R} \frac{\partial w}{\partial \phi} - \frac{v}{R} \right) \end{aligned} \right] R dx d\phi dz \quad (27) \end{aligned}$$

Besides, the following equation shows the variation of kinetic energy:

$$\delta K = \int_{-\frac{h}{2}}^{\frac{h}{2}} \int_0^{2\pi} \int_0^L \rho(z) \left[ \left( \frac{\partial \delta u_x}{\partial t} \right)^2 + \left( \frac{\partial \delta u_\phi}{\partial t} \right)^2 + \left( \frac{\partial \delta u_z}{\partial t} \right)^2 \right] R dx d\phi dz \quad (28)$$

Eventually, the work done's variation by external loads can be computed by the following equation:

$$\delta W_{nc} = \int_{-\frac{h}{2}}^{\frac{h}{2}} \int_0^{2\pi} \int_0^L \left( N_1^T \frac{\partial w}{\partial x} + N_2^T \frac{\partial v}{\partial x} \right) \delta w R dx d\phi dz \quad (29)$$

where  $N_1^T$  and  $N_2^T$  denote the thermal loading resultants and it shall be noted that both thermal resultants are equal and can be calculated as:

$$N_1^T = N_2^T = N^T = \int_{-\frac{h}{2}}^{\frac{h}{2}} \frac{2\mu(1+\nu)}{1-\nu} \alpha(z) \Delta T dz \quad (30)$$

in which, temperature change equals  $\Delta T = T - T_0$  and  $T_0$  is reference temperature which is considered to be room temperature. Furthermore,  $\mu$  stands for Lamé parameter. Thus, to achieve the equations of motion of the shell, Equations (27)–(29) shall be substituted in Equation (26):

$$\frac{\partial N_{xx}}{\partial x} + \frac{1}{R} \frac{\partial N_{x\phi}}{\partial \phi} = I_0 \frac{\partial^2 u}{\partial t^2} + I_1 \frac{\partial^2 \theta_x}{\partial t^2} \quad (31)$$

$$\frac{\partial N_{x\phi}}{\partial x} + \frac{1}{R} \frac{\partial N_{\phi\phi}}{\partial \phi} + \frac{Q_{z\phi}}{R} - N^T \frac{\partial^2 v}{\partial x^2} = I_0 \frac{\partial^2 v}{\partial t^2} + I_1 \frac{\partial^2 \theta_\phi}{\partial t^2} \quad (32)$$

$$\frac{\partial Q_{xz}}{\partial x} + \frac{1}{R} \frac{\partial Q_{z\phi}}{\partial \phi} - \frac{N_{\phi\phi}}{R} - N^T \frac{\partial^2 w}{\partial x^2} = I_0 \frac{\partial^2 w}{\partial t^2} \quad (33)$$

$$\frac{\partial M_{xx}}{\partial x} + \frac{1}{R} \frac{\partial M_{x\phi}}{\partial \phi} - Q_{xz} = I_1 \frac{\partial^2 u}{\partial t^2} + I_2 \frac{\partial^2 \theta_x}{\partial t^2} \quad (34)$$

$$\frac{\partial M_{x\phi}}{\partial x} + \frac{1}{R} \frac{\partial M_{\phi\phi}}{\partial \phi} - Q_{\phi z} = I_1 \frac{\partial^2 v}{\partial t^2} + I_2 \frac{\partial^2 \theta_\phi}{\partial t^2} \quad (35)$$

in which, force and momentum resultants can be expressed as:

$$\begin{bmatrix} N_{xx} \\ N_{\phi\phi} \\ N_{x\phi} \end{bmatrix} = \int_{-\frac{h}{2}}^{\frac{h}{2}} \begin{bmatrix} \sigma_{xx} \\ \sigma_{\phi\phi} \\ \sigma_{x\phi} \end{bmatrix} dz \quad (36)$$

$$\begin{bmatrix} M_{xx} \\ M_{\phi\phi} \\ M_{x\phi} \end{bmatrix} = \int_{-\frac{h}{2}}^{\frac{h}{2}} z \begin{bmatrix} \sigma_{xx} \\ \sigma_{\phi\phi} \\ \sigma_{x\phi} \end{bmatrix} dz \quad (37)$$

$$\begin{bmatrix} Q_{xz} \\ Q_{z\phi} \end{bmatrix} = \kappa_s \int_{-\frac{h}{2}}^{\frac{h}{2}} \begin{bmatrix} \sigma_{xz} \\ \sigma_{z\phi} \end{bmatrix} dz \quad (38)$$



where  $\kappa_s$  denotes the shear correction factor considered as 5/6. Also, mass inertias can be stated as follow:

$$\begin{bmatrix} I_0 \\ I_1 \\ I_2 \end{bmatrix} = \int_{-\frac{h}{2}}^{\frac{h}{2}} \rho(z) \begin{bmatrix} 1 \\ z \\ z^2 \end{bmatrix} dz \quad (39)$$

Integrating Equations (36)–(38) over the thickness of the shell, the following relations will be computed:

$$N_{xx} = A_{11} \frac{\partial u}{\partial x} + B_{11} \frac{\partial \theta_x}{\partial x} + \frac{A_{12}}{R} \left( \frac{\partial v}{\partial \phi} + w \right) + \frac{B_{12}}{R} \frac{\partial \theta_\phi}{\partial \phi} \quad (40)$$

$$N_{x\phi} = A_{66} \left( \frac{1}{R} \frac{\partial u}{\partial \phi} + \frac{\partial v}{\partial x} \right) + B_{66} \left( \frac{1}{R} \frac{\partial \theta_x}{\partial \phi} + \frac{\partial \theta_\phi}{\partial x} \right) \quad (41)$$

$$N_{\phi\phi} = A_{12} \frac{\partial u}{\partial x} + B_{12} \frac{\partial \theta_x}{\partial x} + \frac{A_{11}}{R} \left( \frac{\partial v}{\partial \phi} + w \right) + \frac{B_{11}}{R} \frac{\partial \theta_\phi}{\partial \phi} \quad (42)$$

$$M_{xx} = B_{11} \frac{\partial u}{\partial x} + D_{11} \frac{\partial \theta_x}{\partial x} + \frac{B_{12}}{R} \left( \frac{\partial v}{\partial \phi} + w \right) + \frac{D_{12}}{R} \frac{\partial \theta_\phi}{\partial \phi} \quad (43)$$

$$M_{x\phi} = B_{66} \left( \frac{1}{R} \frac{\partial u}{\partial \phi} + \frac{\partial v}{\partial x} \right) + D_{66} \left( \frac{1}{R} \frac{\partial \theta_x}{\partial \phi} + \frac{\partial \theta_\phi}{\partial x} \right) \quad (44)$$

$$M_{\phi\phi} = B_{12} \frac{\partial u}{\partial x} + D_{12} \frac{\partial \theta_x}{\partial x} + \frac{B_{11}}{R} \left( \frac{\partial v}{\partial \phi} + w \right) + \frac{D_{11}}{R} \frac{\partial \theta_\phi}{\partial \phi} \quad (45)$$

$$Q_{xz} = A_{55}^s \left( \theta_x + \frac{\partial w}{\partial x} \right) \quad (46)$$

$$Q_{z\phi} = A_{44}^s \left( \theta_\phi + \frac{1}{R} \frac{\partial w}{\partial \phi} - \frac{v}{R} \right) \quad (47)$$

in which

$$\begin{bmatrix} A_{11} \\ A_{12} \\ A_{66} \end{bmatrix} = \int_{-\frac{h}{2}}^{\frac{h}{2}} \begin{bmatrix} \frac{2\mu}{1-\nu} \\ \frac{2\nu\mu}{1-\nu} \\ \mu \end{bmatrix} dz \quad (48)$$

$$\begin{bmatrix} B_{11} \\ B_{12} \\ B_{66} \end{bmatrix} = \int_{-\frac{h}{2}}^{\frac{h}{2}} z \begin{bmatrix} \frac{2\mu}{1-\nu} \\ \frac{2\nu\mu}{1-\nu} \\ \mu \end{bmatrix} dz \quad (49)$$

$$\begin{bmatrix} D_{11} \\ D_{12} \\ D_{66} \end{bmatrix} = \int_{-\frac{h}{2}}^{\frac{h}{2}} z^2 \begin{bmatrix} \frac{2\mu}{1-\nu} \\ \frac{2\nu\mu}{1-\nu} \\ \mu \end{bmatrix} dz \quad (50)$$

$$A_{44}^s = A_{55}^s = \kappa_s \int_{-\frac{h}{2}}^{\frac{h}{2}} \mu dz \quad (51)$$

Finally, by inserting Equations (40)–(47) into Equations (31)–(35) and also performing simplification, the governing equations of imperfect metal foam shell will be calculated:

$$A_{11} \frac{\partial^2 u}{\partial x^2} + B_{11} \frac{\partial^2 \theta_x}{\partial x^2} + \frac{A_{12}}{R} \left( \frac{\partial^2 v}{\partial x \partial \phi} + \frac{\partial w}{\partial x} \right) + \frac{B_{12}}{R} \frac{\partial^2 \theta_\phi}{\partial x \partial \phi} + \frac{A_{66}}{R} \left( \frac{1}{R} \frac{\partial^2 u}{\partial \phi^2} + \frac{\partial^2 v}{\partial x \partial \phi} \right) + \frac{B_{66}}{R} \left( \frac{1}{R} \frac{\partial^2 \theta_x}{\partial \phi^2} + \frac{\partial^2 \theta_\phi}{\partial x \partial \phi} \right) - l_0 \frac{\partial^2 u}{\partial t^2} - l_1 \frac{\partial^2 \theta_x}{\partial t^2} = 0 \quad (52)$$

$$A_{66} \left( \frac{1}{R} \frac{\partial^2 u}{\partial x \partial \phi} + \frac{\partial^2 v}{\partial x^2} \right) + B_{66} \left( \frac{1}{R} \frac{\partial^2 \theta_x}{\partial x \partial \phi} + \frac{\partial^2 \theta_\phi}{\partial x^2} \right) + \frac{A_{12}}{R} \frac{\partial^2 u}{\partial x \partial \phi} + \frac{B_{12}}{R} \frac{\partial^2 \theta_\phi}{\partial x \partial \phi} + \frac{A_{11}}{R^2} \left( \frac{\partial^2 v}{\partial \phi^2} + \frac{\partial w}{\partial \phi} \right) + \frac{B_{11}}{R^2} \frac{\partial^2 \theta_\phi}{\partial \phi^2} + \frac{A_{55}^s}{R} \left( \theta_\phi + \frac{1}{R} \frac{\partial w}{\partial \phi} - \frac{v}{R} \right) - N^T \frac{\partial^2 v}{\partial x^2} - l_0 \frac{\partial^2 v}{\partial t^2} - l_1 \frac{\partial^2 \theta_\phi}{\partial t^2} = 0 \quad (53)$$

$$A_{55}^s \left( \frac{\partial \theta_x}{\partial x} + \frac{\partial^2 w}{\partial x^2} \right) + \frac{A_{55}^s}{R} \left( \frac{\partial \theta_\phi}{\partial \phi} + \frac{1}{R} \frac{\partial^2 w}{\partial \phi^2} - \frac{1}{R} \frac{\partial v}{\partial \phi} \right) - \frac{A_{12}}{R} \frac{\partial u}{\partial x} - \frac{B_{12}}{R} \frac{\partial \theta_x}{\partial x} - \frac{A_{11}}{R^2} \left( \frac{\partial v}{\partial \phi} + w \right) - \frac{B_{11}}{R^2} \frac{\partial \theta_\phi}{\partial \phi} - N^T \frac{\partial^2 w}{\partial x^2} - l_0 \frac{\partial^2 w}{\partial t^2} = 0 \quad (54)$$

$$B_{11} \frac{\partial^2 u}{\partial x^2} + D_{11} \frac{\partial^2 \theta_x}{\partial x^2} + \frac{B_{12}}{R} \left( \frac{\partial^2 v}{\partial x \partial \phi} + \frac{\partial w}{\partial x} \right) + \frac{D_{12}}{R} \frac{\partial^2 \theta_\phi}{\partial x \partial \phi} + \frac{B_{66}}{R} \left( \frac{1}{R} \frac{\partial^2 u}{\partial \phi^2} + \frac{\partial^2 v}{\partial x \partial \phi} \right) + \frac{D_{66}}{R} \left( \frac{1}{R} \frac{\partial^2 \theta_x}{\partial \phi^2} + \frac{\partial^2 \theta_\phi}{\partial x \partial \phi} \right) - A_{55}^s \left( \theta_x + \frac{\partial w}{\partial x} \right) - l_1 \frac{\partial^2 u}{\partial t^2} - l_2 \frac{\partial^2 \theta_x}{\partial t^2} = 0 \quad (55)$$

$$B_{66} \left( \frac{1}{R} \frac{\partial^2 u}{\partial x \partial \phi} + \frac{\partial^2 v}{\partial x^2} \right) + D_{66} \left( \frac{1}{R} \frac{\partial^2 \theta_x}{\partial x \partial \phi} + \frac{\partial^2 \theta_\phi}{\partial x^2} \right) + \frac{B_{12}}{R} \frac{\partial^2 u}{\partial x \partial \phi} + \frac{D_{12}}{R} \frac{\partial^2 \theta_\phi}{\partial x \partial \phi} + \frac{B_{11}}{R^2} \left( \frac{\partial^2 v}{\partial \phi^2} + \frac{\partial w}{\partial \phi} \right) + \frac{D_{11}}{R^2} \frac{\partial^2 \theta_\phi}{\partial \phi^2} - A_{55}^s \left( \theta_\phi + \frac{1}{R} \frac{\partial w}{\partial \phi} - \frac{v}{R} \right) - l_1 \frac{\partial^2 v}{\partial t^2} - l_2 \frac{\partial^2 \theta_\phi}{\partial t^2} = 0 \quad (56)$$

A harmonic solution is implemented in order to solve the obtained governing equations of imperfect metal foam shells. Thus, the displacement fields were supposed in the following form [47]:

$$\begin{Bmatrix} u \\ v \\ w \\ \theta_x \\ \theta_\phi \end{Bmatrix} = \begin{Bmatrix} U_n \\ V_n \\ W_n \\ \Theta_{xn} \\ \Theta_{\phi n} \end{Bmatrix} e^{(i\beta x + in\phi - i\omega_n t)} \quad (57)$$

In the above equation,  $U$ ,  $V$  and  $W$  represents the amplitudes of displacements, respectively, while  $\theta_x$  and  $\theta_\phi$  denotes rotation amplitudes, respectively. Plus,  $\beta$  represents the longitudinal wavenumber and  $n$  represents the circumferential wave number. Also,  $\omega_n$  is the circular frequency and  $i = \sqrt{-1}$  is the imaginary unit. In this case, the simply-supported boundary condition is taken into account. Next, by replacing Equation (57) into Equations

(52)–(56), the following equation can be attained:

$$([K - \omega_n^2 M]_{5 \times 5}) \begin{bmatrix} U_n \\ V_n \\ W_n \\ \Theta_{xn} \\ \Theta_{\phi n} \end{bmatrix} = 0 \quad (58)$$

in which  $K$  represents stiffness matrix and  $M$  represents mass matrix. The elements of such matrices are provided in the Appendix.

The determinant of the coefficient matrix of Equation (58) shall be set to zero to solve such eigenvalue problem and calculate the value of natural frequency:

$$|[K - \omega_n^2 M]_{5 \times 5}| = 0 \quad (59)$$

By dividing the circular frequency by  $2\pi$ , the wave frequency will be calculated. Besides, by setting  $\beta = n = \eta$ , the phase velocity will be computed as follow:

$$c_{Phase} = \frac{\omega_n}{\eta} \quad (60)$$

## Numerical findings and discussion

In the current part, several diagrams are presented to clarify the influence of different parameters on the wave propagation behavior of metal foam circular cylindrical shells. In this research, the thickness of the shell was assumed to be 3 cm; also, both the length and radius of the shell were taken 40 times greater than the shell's thickness. The mechanical properties of the material at room temperature ( $T = 300$  K) are presented in Table 1.

First of all, the introduced methodology was validated by comparing the presented outcomes with those stated by Pradhan, Loy [48], Wang and Wu [14] and Li, Pang [49]. According to Table 2, there is an acceptable consistency between the results of the presented method and those reported by previous investigations.

Figure 3 reveals the changes in wave frequency as a function of circumferential wave numbers for various types of porosity distribution. According to this diagram, it can be inferred that theoretically, SPD metal foam structures are the best choice in various industries since SPD experiences the highest wave frequency followed by ASPD and UPD, respectively. This result should be examined experimentally. Manufacturing metal foam with SPD can be a challenging task. Besides, the circumferential wave number had an increasing influence on the variation of wave frequency in the circular cylindrical metal foam shell.

**Table 1.** Mechanical properties of Ti-6Al-4V foam at room temperature.

Mechanical properties	Value
$E_1$ (GPa)	105.7
$\nu$	0.2981
$\rho_1$ (Kg/m <sup>3</sup> )	4429
$\alpha_1$ ( $\mu$ /K)	6.941

**Table 2.** Comparison of the dimensionless natural frequency  $\left(\Omega = \omega R \sqrt{\frac{\rho}{E(1-\nu^2)}}\right)$  of the cylindrical shell for the C-C boundary condition.

$N$	Pradhan, Loy [48]	Wang and Wu [14]	Li, Pang [49]	Present
1	0.0342	0.0340	0.0332	0.0351
2	0.0119	0.0119	0.0117	0.0122
3	0.0072	0.0072	0.0071	0.0072
4	0.0089	0.0090	0.0090	0.0089
5	0.0136	0.0137	0.0137	0.0135

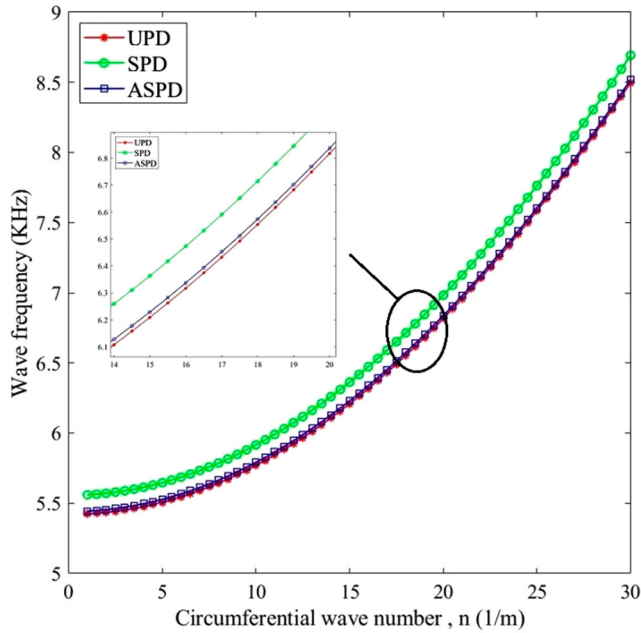


**Figure 3.** Illustration of variation of wave frequency as a function of circumferential wave number for various types of porosity distribution through the thickness of the shell.

The effect of different types of porosity distribution through the shell thickness on phase velocity is demonstrated in Figure 4 as a function of circumferential wave number. A decreasing trend can be observed with different slopes. At lower circumferential wave numbers, curves or values of phase velocity decreased with a steep slope; while at greater circumferential wave numbers, this decrease occurred at milder slopes. Furthermore, based on the magnified diagram, it can be understood that the lower effects on the phase velocity can be observed in the case of SPD as higher phase velocity happened in SPD. Also, UPD has the greatest negative effect on the phase velocity values as compared to ASPD and SPD.

The effects of both the porosity coefficient and porosity distribution on the variation of phase velocity are illustrated in Figure 5. As can be seen, the phase velocity is inversely proportional to the porosity coefficient. In other words, the presence of pores weakens the structure and declines its stiffness; hence the non-porous structure can tolerate greater

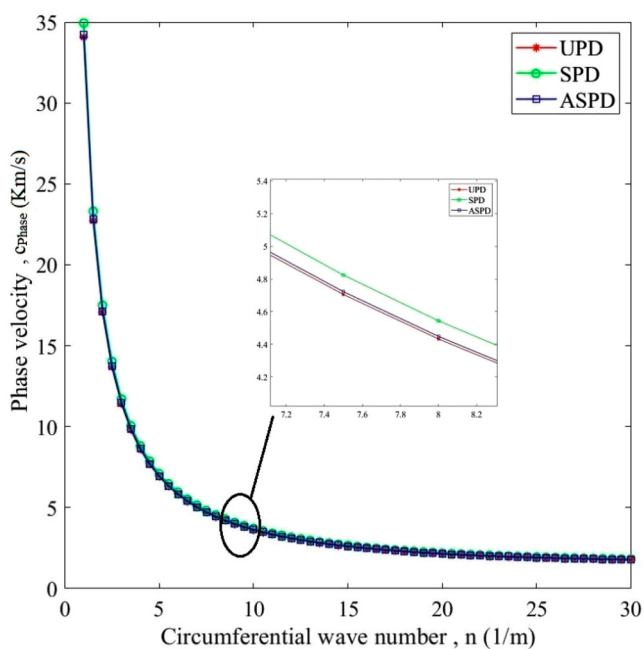


**Figure 4.** The effect of different types of porosity distribution through the shell thickness on changes of phase velocity against the circumferential wave number.

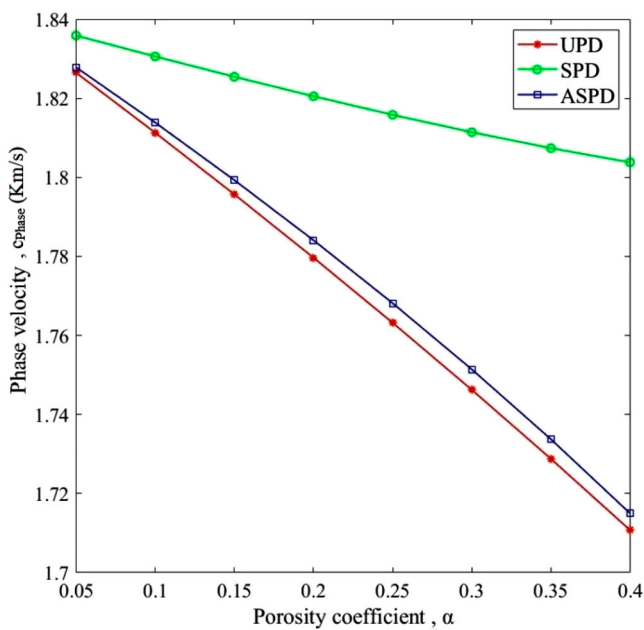


**Figure 5.** Variation of phase velocity against porosity coefficient for different kinds of porosity distribution through the thickness of the shell.

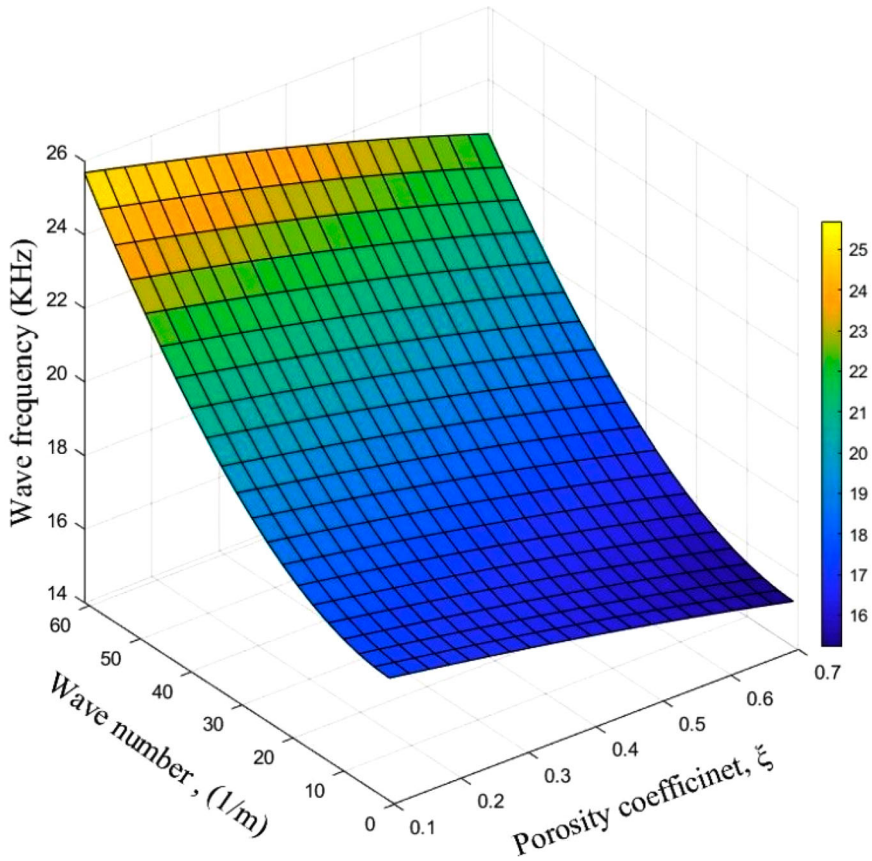


**Figure 6.** Variation of wave frequency against wave number for various amounts of porosity coefficient.

phase velocity than the porous one. Furthermore, the SPD corresponds to greater phase velocity values.

Figure 6 indicates the influence of the porosity coefficient on the variation of wave frequency as a function of the circumferential wave number. At a certain circumferential wave number, an increment in the porosity coefficient declined the wave frequency, moreover, it can be seen that the circumferential wave number possesses an increasing influence on wave frequency. Porosity is an unavoidable phenomenon during the manufacturing process. This phenomenon is also known as a defect and can negatively affect the mechanical performance of structures. This can explain the trend of this diagram in which the wave frequency decreased by augmentation of the porosity coefficient.

Variations of phase velocity by the circumferential wave number are plotted in Figure 7 for different porosity coefficients. As shown, the curves exhibited an initial dramatic decrease followed by a gradually decrementing slope by the further increment of the circumferential wave number. For further elucidation of the impact of the porosity coefficient on the phase velocity, a more accurate magnifier was utilized. According to the magnified diagram, the porosity coefficient influenced the phase velocity value similar to the case of

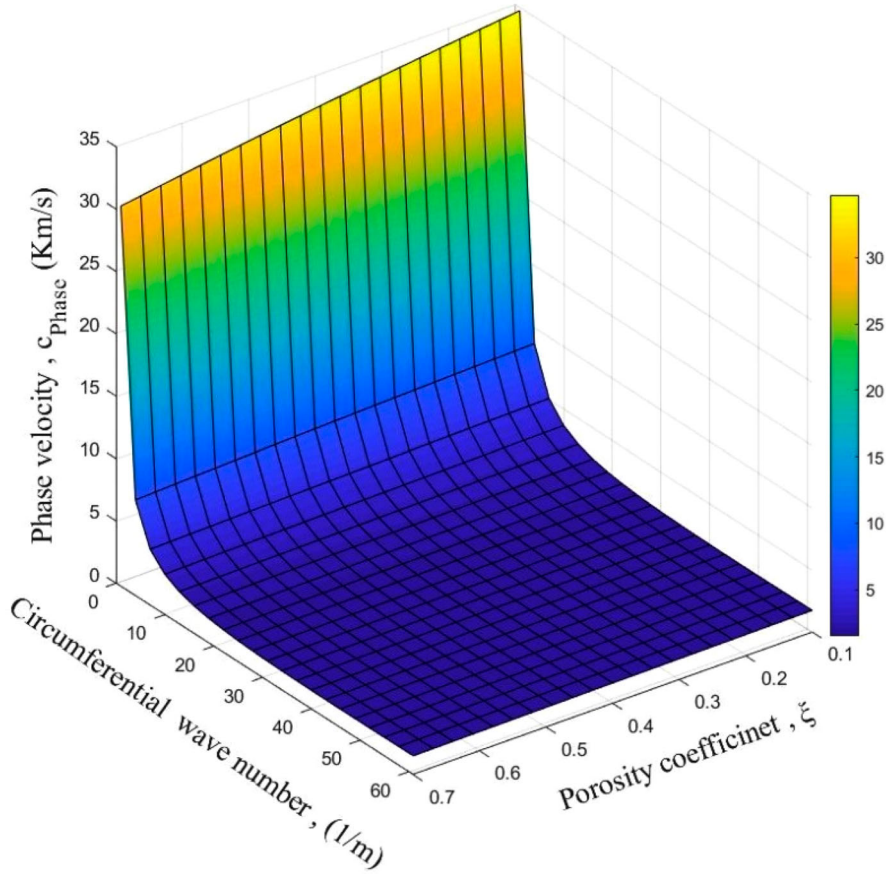


**Figure 7.** The influence of porosity coefficient on the variation of phase velocity against the circumferential wave number.

the wave frequency: the phase velocity values were reduced by an increment of the porosity coefficient.

Figure 8 demonstrates the effect of radius to thickness ratio on the variation of phase velocity for different porosity coefficients. As observed, the curves have a descending trend. In other words, the radius to thickness ratio caused a decreasing effect on the variation of phase velocity. This could be ascribed to the softening influence of radius to thickness ratio increment and the decline of the structure stiffness by the growth of this ratio. As mentioned before, increasing the porosity coefficient decreases phase velocity.

Figure 9 is drawn to probe the effect of temperature change on the variation of wave frequency versus circumferential wave number for (a) SPD, (b) ASPD and (c) UPD. Based on these diagrams, it can be realized that temperature change possesses a negative effect on the value of wave frequency. That is, the value of wave frequency will be reduced with increasing temperature change value. The corresponding reason for this behavior is that the stiffness of the structure will be lessened, i.e. the structure becomes weaker by rising temperature change amount. Moreover, by comparing plotted diagrams, it is clear that their trends are similar and by rising circumferential wave number, wave frequency value

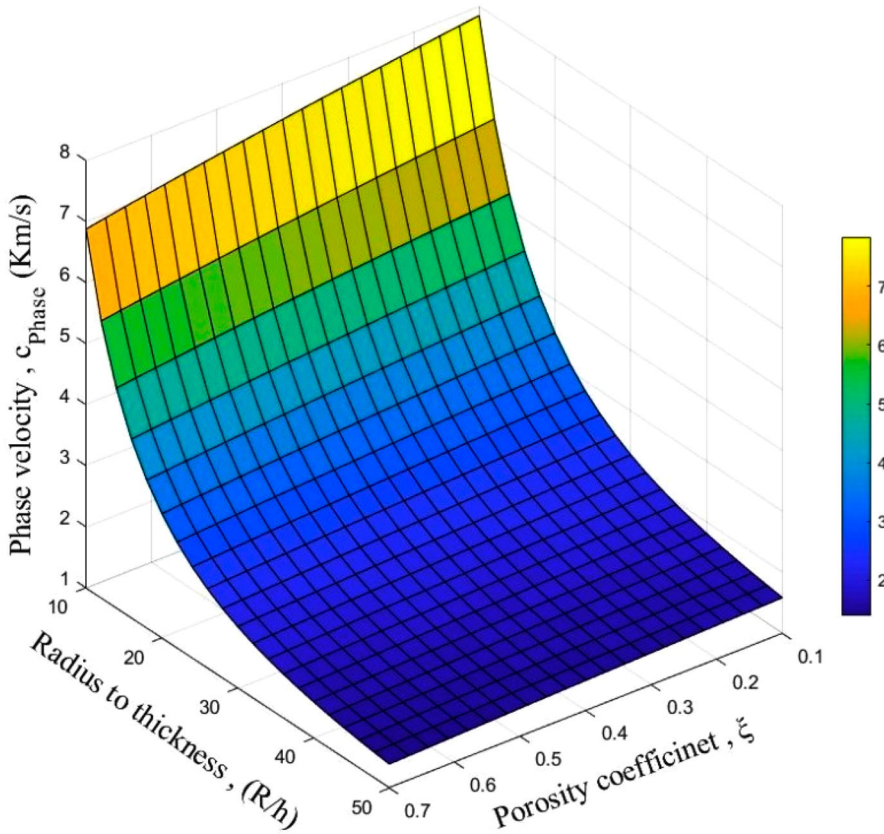


**Figure 8.** Variation of phase velocity against radius to thickness ratio for different amounts of porosity coefficients.

grows. However, they are different in terms of values: SPD, ASPD and UPD have the greatest values, respectively.

In Figures 10 and 11, the effect of various kinds of temperature variation on changes of wave frequency and phase velocity values versus temperature change for (a) the first mode, (b) the second mode and (c) the third mode, respectively. According to this figure, it can be understood that wave frequency and phase velocity values experience higher values at higher frequency modes. Besides, the decreasing effect of temperature change which was mentioned in the discussion of Figure 9 is also observed in these diagrams. From these figures, we can see how various kinds of temperature variations affect values of wave frequency and phase velocity. As observed, STV has the least negative influence on the variation of wave frequency and phase velocity and inversely, UTV has the most negative effect on wave frequency and phase velocity values by rising temperature change amount.

### Concluding remarks

The present investigation was aimed to assess wave propagation in a porous metal foam circular cylindrical shell in a thermal environment. To this end, FSDT and Hamilton's principle were employed to obtain the governing equations. Various porosity distribution



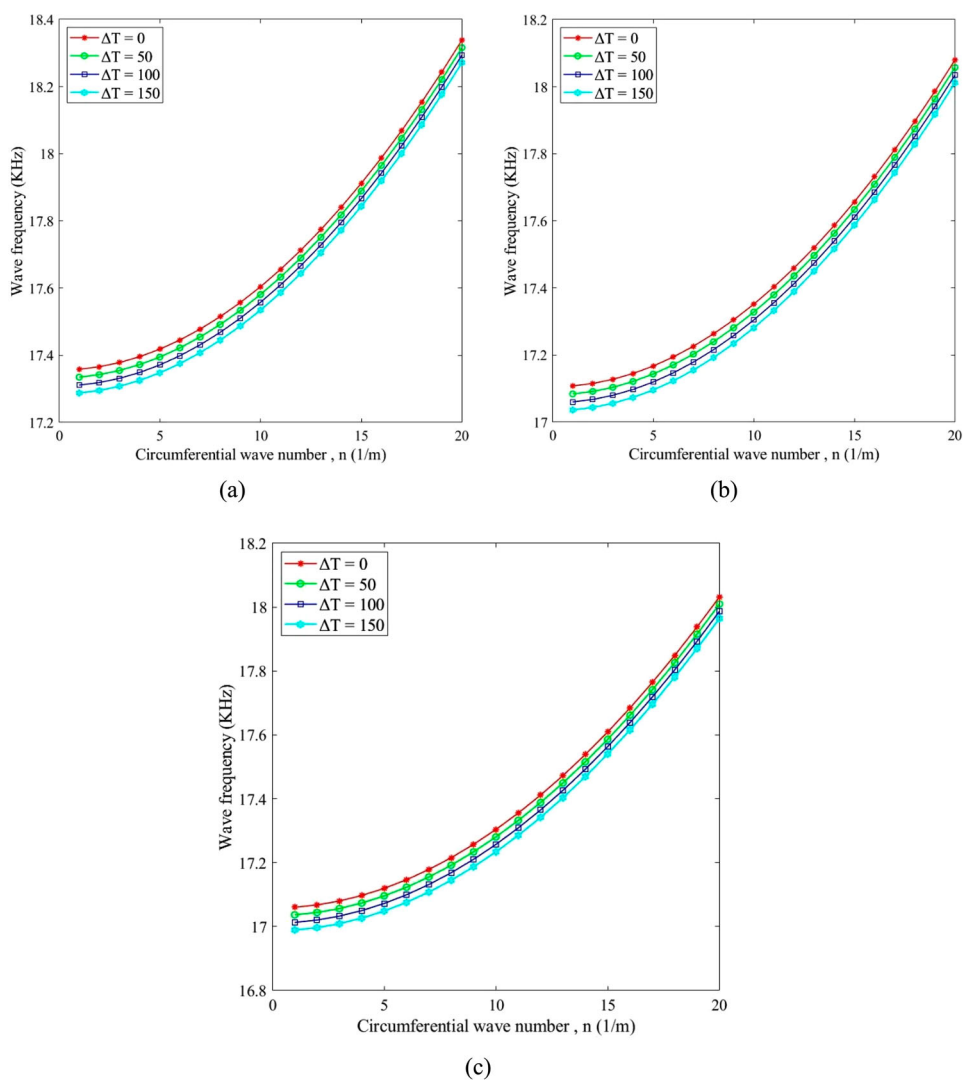


**Figure 9.** Illustration of variation of wave frequency versus circumferential wave number for various temperature changes for (a) SPD, (b) ASPD and (c) UPD.

patterns were considered through the shell thickness. Also, various types of variation of temperatures such as STV, LTV and UTV were surveyed. Eventually, the obtained governing equations were analytically solved. The most remarkable highlights are expressed in the following.

We observed that the phase velocity and wave frequency of the porous metal foam circular cylindrical shell decrease with the elevation of porosity coefficient, and an increment in the radius to thickness ratio has a decreasing effect on the phase velocity. Also, the SPD and UPD models can tolerate the highest and lowest phase velocity and wave frequency, respectively, and higher values of phase velocity and wave frequency are associated with higher circumferential wave numbers. Finally, we concluded that temperature change has

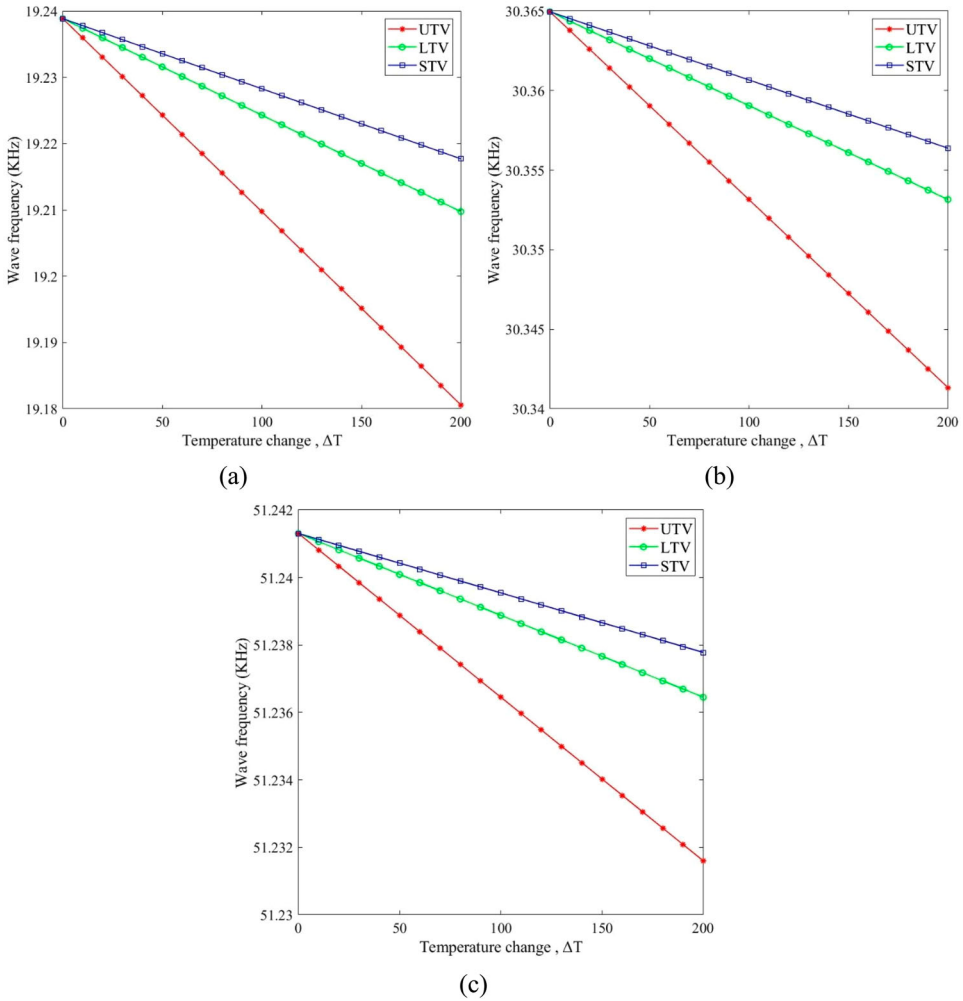


**Figure 10.** Illustration of variation of wave frequency versus temperature change for various kinds of temperature variation for (a) first mode, (b) second mode and (c) third mode.

a decreasing effect on the variation of wave frequency values. In other words, the value of wave frequency will be reduced with increasing temperature change value, as the stiffness of the structure will be decreased. Comparing the resulted curves demonstrated that the variation of wave frequency versus circumferential wave number for various temperature changes for SPD, ASPD and UPD are qualitatively similar, with SPD and UPD having the largest and smallest values, respectively. Also, the influence of various types of temperature variation was investigated. Based on the presented diagrams, it can be figured out that a thermal environment in which temperature varies according to a sinusoidal model has a less decreasing effect on the variations of wave frequency and phase velocity compared to the linear and uniform models. On the other hand, greater wave frequencies and phase velocities happen in thermal environments with STV, LTV and UTV, respectively. Furthermore, wave frequency and phase velocity values become greater with the growth of mode number.

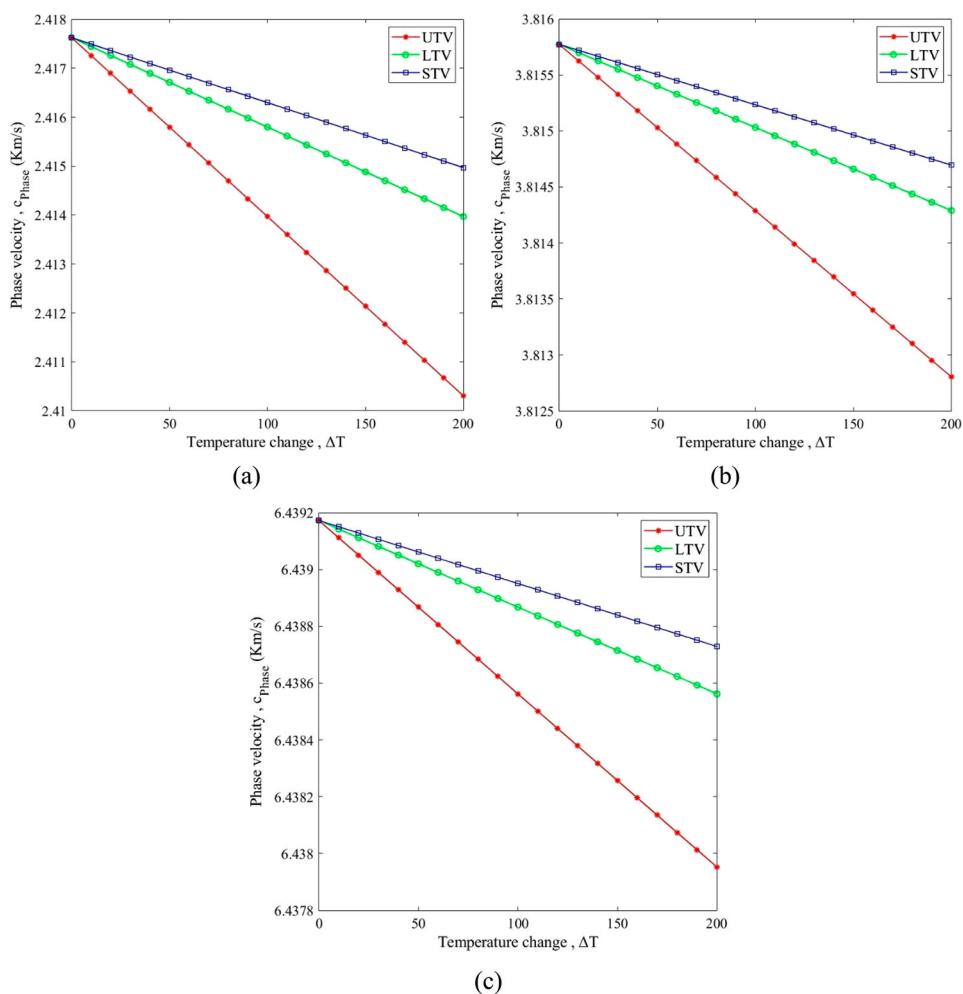


**Figure 11.** Variation of phase velocity versus temperature change for various kinds of temperature variation for the (a) first mode, (b) second mode, and (c) third mode.

## Disclosure statement

No potential conflict of interest was reported by the author(s).

## Funding

This research is financially supported by the Department of Science and Technology of Shandong Province (Grant No. 2021CXGC011204), the Taishan Scholar Priority Discipline Talent Group program funded by the Shandong Province, and the first-class discipline project funded by the Education Department of Shandong Province.

## References

- [1] Banhart J. Manufacture, characterisation and application of cellular metals and metal foams. *Prog Mater Sci.* **2001**;46(6):559–632.
- [2] Smith B, Szyniszewski S, Hajjar J, et al. Steel foam for structures: a review of applications, manufacturing and material properties. *J Constr Steel Res.* **2012**;71:1–10.
- [3] Rakow JF, Waas AM. Thermal buckling of metal foam sandwich panels for convective thermal protection systems. *J Spacecr Rockets.* **2005**;42(5):832–844.
- [4] Magnucka-Blandzi E. Dynamic stability of a metal foam circular plate. *J Theor Appl Mech.* **2009**;47:421–433.
- [5] Belica T, Malinowski M, Magnucki K. Dynamic stability of an isotropic metal foam cylindrical shell subjected to external pressure and axial compression. *J Appl Mech.* **2011**;78:4. DOI:[10.1115/1.4003768](https://doi.org/10.1115/1.4003768)
- [6] Karami B, Shahsavari D, Janghorban M. On the dynamics of porous doubly-curved nanoshells. *Int J Eng Sci.* **2019**;143:39–55.
- [7] Karami B, Janghorban M, Rabczuk T. Dynamics of two-dimensional functionally graded tapered Timoshenko nanobeam in thermal environment using nonlocal strain gradient theory. *Composites Part B: Engineering.* **2020**;182:107622. DOI:[10.1016/j.compositesb.2019.107622](https://doi.org/10.1016/j.compositesb.2019.107622)
- [8] Karami B, Shahsavari D, Janghorban M, et al. Free vibration analysis of FG nanoplate with porous imperfection in hygrothermal environment. *Struct Eng Mech.* **2020**;73(2): 191–207.
- [9] Dunand DC. Processing of titanium foams. *Adv Eng Mater.* **2004**;6(6):369–376.
- [10] Murray N, Dunand DC. Microstructure evolution during solid-state foaming of titanium. *Compos Sci Technol.* **2003**;63(16):2311–2316.
- [11] Esen Z, Bor Ş. Characterization of Ti–6Al–4V alloy foams synthesized by space holder technique. *Mater Sci Eng A.* **2011**;528(7-8):3200–3209.
- [12] Chen D, Yang J, Kitipornchai S. Elastic buckling and static bending of shear deformable functionally graded porous beam. *Compos Struct.* **2015**;133:54–61.
- [13] Chen D, Yang J, Kitipornchai S. Free and forced vibrations of shear deformable functionally graded porous beams. *Int J Mech Sci.* **2016**;108-109:14–22.
- [14] Wang Y, Wu D. Free vibration of functionally graded porous cylindrical shell using a sinusoidal shear deformation theory. *Aerosp Sci Technol.* **2017**;66:83–91.
- [15] Kitipornchai S, Chen D, Yang J. Free vibration and elastic buckling of functionally graded porous beams reinforced by graphene platelets. *Mater Des.* **2017**;116:656–665.
- [16] Barati MR. Nonlocal-strain gradient forced vibration analysis of metal foam nanoplates with uniform and graded porosities. *Adv Nano Res.* **2017**;5(4):393–414.
- [17] Barati MR, Zenkour AM. Investigating post-buckling of geometrically imperfect metal foam nanobeams with symmetric and asymmetric porosity distributions. *Compos Struct.* **2017**;182: 91–98.
- [18] Yang J, Chen D, Kitipornchai S. Buckling and free vibration analyses of functionally graded graphene reinforced porous nanocomposite plates based on Chebyshev-Ritz method. *Compos Struct.* **2018**;193:281–294.
- [19] Wang Y, Zhang Z. Non-local buckling analysis of functionally graded nanoporous metal foam nanoplates. *Coatings.* **2018**;8(11):389. DOI:[10.3390/coatings8110389](https://doi.org/10.3390/coatings8110389)
- [20] Gao K, Gao W, Chen D, et al. Nonlinear free vibration of functionally graded graphene platelets reinforced porous nanocomposite plates resting on elastic foundation. *Compos Struct.* **2018**;204:831–846.
- [21] Dong Y, Li Y, Chen D, et al. Vibration characteristics of functionally graded graphene reinforced porous nanocomposite cylindrical shells with spinning motion. *Compos B Eng.* **2018**;145:1–13.
- [22] Fenjan RM, Ahmed RA, Alasadi AA, et al. Nonlocal strain gradient thermal vibration analysis of double-coupled metal foam plate system with uniform and non-uniform porosities. *Coupled Syst Mech.* **2019**;8(3):247–257.
- [23] Wang YQ, Ye C, Zu JW. Nonlinear vibration of metal foam cylindrical shells reinforced with graphene platelets. *Aerosp Sci Technol.* **2019**;85:359–370.

- [24] Wang YQ, Liu YF, Zu JW. On scale-dependent vibration of circular cylindrical nanoporous metal foam shells. *Microsyst Technol.* 2019;25(7):2661–2674.
- [25] Mirjavadi SS, Forsat M, Barati MR, et al. Dynamic response of metal foam FG porous cylindrical micro-shells due to moving loads with strain gradient size-dependency. *Eur Phys J Plus.* 2019;134(5):214. DOI:10.1140/epjp/i2019-12540-3
- [26] Zhang Y, Zhang F. Vibration and buckling of shear deformable functionally graded nanoporous metal foam nanoshells. *Nanomaterials.* 2019;9(2):271. DOI:10.3390/nano9020271
- [27] Alasadi AA, Ahmed RA, Faleh NM. Analyzing nonlinear vibrations of metal foam nanobeams with symmetric and non-symmetric porosities. *Adv Aircr Spacecr.* 2019;6(4):273–282.
- [28] Liu Y, Wang Y. Size-dependent free vibration and buckling of three-dimensional graphene foam microshells based on modified couple stress theory. *Materials.* 2019;12(5):729. DOI:10.3390/ma12050729
- [29] Ebrahimi F, Seyfi A. Studying propagation of wave of metal foam rectangular plates with graded porosities resting on Kerr substrate in thermal environment via analytical method. *Waves Random Compl Media.* 2020: 1–24. DOI:10.1080/17455030.2020.1802531
- [30] Karami B, Janghorban M, Tounsi A. Wave propagation of functionally graded anisotropic nanoplates resting on Winkler-Pasternak foundation. *Struct Eng Mech.* 2019;70(1):55–66.
- [31] Karami B, Janghorban M, Tounsi A. Variational approach for wave dispersion in anisotropic doubly-curved nanoshells based on a new nonlocal strain gradient higher order shell theory. *Thin Walled Struct.* 2018;129:251–264.
- [32] Karami B, Shahsavari D, Janghorban M. Wave propagation analysis in functionally graded (FG) nanoplates under in-plane magnetic field based on nonlocal strain gradient theory and four variable refined plate theory. *Mech Adv Mater Struct.* 2018;25(12):1047–1057.
- [33] Ebrahimi F, Dehghan M, Seyfi A. Eringen's nonlocal elasticity theory for wave propagation analysis of magneto-electro-elastic nanotubes. *Adv Nano Res.* 2019;7(1):1–11.
- [34] Karami B, Shahsavari D, Li L. Hygrothermal wave propagation in viscoelastic graphene under in-plane magnetic field based on nonlocal strain gradient theory. *Phys E Low Dimens Syst Nanostruct.* 2018;97:317–327.
- [35] She G-L, Yuan F-G, Ren Y-R. On wave propagation of porous nanotubes. *Int J Eng Sci.* 2018;130:62–74.
- [36] Ayache B, Bennai R, Fahsi B, et al. Analysis of wave propagation and free vibration of functionally graded porous material beam with a novel four variable refined theory. *Earthq Struct.* 2018;15(4):369–382.
- [37] Karami B, Shahsavari D, Li L. Temperature-dependent flexural wave propagation in nanoplate-type porous heterogeneous material subjected to in-plane magnetic field. *J Therm Stresses.* 2018;41(4):483–499.
- [38] Ebrahimi F, Seyfi A, Dabbagh A. A novel porosity-dependent homogenization procedure for wave dispersion in nonlocal strain gradient inhomogeneous nanobeams. *Eur Phys J Plus.* 2019;134(5):226. DOI:10.1140/epjp/i2019-12547-8
- [39] Ebrahimi F, Seyfi A, Dabbagh A. Dispersion of waves in FG porous nanoscale plates based on NSGT in thermal environment. *Adv Nano Res.* 2019;7(5):325–335.
- [40] Wang YQ, Liang C. Wave propagation characteristics in nanoporous metal foam nanobeams. *Results Phys.* 2019;12:287–297.
- [41] Sobhy M, Zenkour AM. Wave propagation in magneto-porosity FG bi-layer nanoplates based on a novel quasi-3D refined plate theory. *Waves Random Compl Media.* 2019: 1–21. DOI:10.1080/17455030.2019.1634853
- [42] Faroughi S, Rahmani A, Friswell M. On wave propagation in two-dimensional functionally graded porous rotating nano-beams using a general nonlocal higher-order beam model. *Appl Math Model.* 2020;80:169–190.
- [43] Ebrahimi F, Dabbagh A, Rastgoo A. Vibration analysis of porous metal foam shells rested on an elastic substrate. *J Strain Anal Eng Design.* 2019;54(3):199–208.
- [44] Ebrahimi F, Seyfi A. Studying propagation of wave in metal foam cylindrical shells with graded porosities resting on variable elastic substrate. *Eng Comput.* 2020. DOI:10.1007/s00366-020-01069-w

- [45] Cheshmeh E, Karbon M, Eyvazian A, et al. Buckling and vibration analysis of FG-CNTRC plate subjected to thermo-mechanical load based on higher order shear deformation theory. *Mech Based Des Struct Mach.* 2020; 1–24. DOI:10.1080/15397734.2020.1744005
- [46] Ebrahimi F, Seyfi A. Propagation of flexural waves in anisotropic fluid-conveying cylindrical shells. *Symmetry.* 2020;12(6):901. DOI:10.3390/sym12060901
- [47] Ebrahimi F, Seyfi A. Wave propagation response of multi-scale hybrid nanocomposite shell by considering aggregation effect of CNTs. *Mech Based Des Struct Mach.* 2019;49(1):59–80.
- [48] Pradhan S, Loy C, Lam K, et al. Vibration characteristics of functionally graded cylindrical shells under various boundary conditions. *Appl Acoust.* 2000;61(1):111–129.
- [49] Li H, Pang F, Chen H, et al. Vibration analysis of functionally graded porous cylindrical shell with arbitrary boundary restraints by using a semi analytical method. *Compos B Eng.* 2019;164:249–264.

## Appendix

The components of stiffness and mass matrices are as follows:

$$\begin{aligned}
 K_{11} &= -A_{11}\beta^2 - \frac{A_{66}}{R^2}n^2, K_{12} = -\beta n\left(\frac{A_{12}+A_{66}}{R}\right), K_{13} = \frac{A_{12}}{R}\beta i, \\
 K_{14} &= -B_{11}\beta^2 - \frac{B_{66}}{R^2}n^2, K_{15} = -\beta n\left(\frac{B_{12}+B_{66}}{R}\right), K_{22} = -A_{66}\beta^2 - \frac{A_{11}}{R^2}n^2 - \frac{A_{55}^s}{R^2} - N^T\beta^2, \\
 K_{23} &= n\left(\frac{A_{11}+A_{55}^s}{R^2}\right)i, K_{24} = -\beta n\left(\frac{B_{12}+B_{66}}{R}\right), K_{25} = -B_{66}\beta^2 - \frac{B_{11}}{R^2}n^2 - \frac{A_{55}^s}{R}, \\
 K_{33} &= -A_{55}^s\beta^2 - \left[\frac{A_{11}}{R^2} + n^2\frac{A_{55}^s}{R^2}\right] - N^T\beta^2, K_{34} = \left(A_{55}^s - \frac{B_{12}}{R}\right)i\beta, K_{35} = n\left(\frac{A_{55}^s}{R} - \frac{B_{11}}{R^2}\right)i, \\
 K_{44} &= -D_{11}\beta^2 - n^2\frac{D_{66}}{R^2} - A_{55}^s, K_{45} = -\beta n\frac{D_{12}+D_{66}}{R}, K_{55} = -D_{66}\beta^2 - n^2\frac{D_{11}}{R^2} - A_{55}^s.
 \end{aligned}$$

$$M_{11} = I_0, M_{14} = I_1, M_{22} = I_0, M_{25} = I_1, M_{33} = I_0, M_{44} = I_2, \text{ and } M_{55} = I_2.$$